BMC Cancer

RESEARCH

Open Access

RBMS1-HSPA8 axis activation drives head and neck squamous cell carcinoma progression

Xinghong Yin[1,2†], Meng Luo[2†], Xiaojun Zha[3], Maoli Duan[4,5*] and Yehai Liu[1*]

Abstract

Background Head and Neck Squamous Cell Carcinoma (HNSCC) presents significant challenges in terms of treatment and prognosis, highlighting the urgent need for new therapeutic targets and the development of effective targeted therapies to enhance patient outcomes and survival.

Methods The expression level of RBMS1 in HNSCC was identified by GEO and TCGA databases through systematic bioinformatics analysis, and further verified in human specimens by quantitative Real-time PCR, Western blot, and immunohistochemistry. The results of CCK-8, colony formation assay, wound healing, Transwell, and tumor formation assays in nude mice showed that RBMS1 promoted the proliferation, migration, and invasion of HNSCC cells. The downstream target genes of RBMS1 were identified in the RBMS1 knockdown and the control groups of TU177 cells using RNA sequencing. HSPA8 was identified as a downstream target gene of RBMS1 in functional in vitro and tumor formation experiments in nude mice.

Results Elevated expression levels of RBMS1 in HNSCC were identified using relevant databases and validated in human specimens. In both in vitro and in vivo studies, overexpression of RBMS1 promoted the proliferation, migration, and invasion of HNSCC cells, whereas knockdown of RBMS1 significantly inhibited these processes. RNA sequencing analysis revealed HSPA8 as a downstream target of RBMS1, and rescue experiments confirmed that HSPA8 serves as a crucial intermediary in the regulatory pathway of tumor progression influenced by RBMS1.

Conclusions This study suggests that RBMS1 regulates HSPA8 to promote the proliferation, migration, and invasion of HNSCC cells, making it a potential therapeutic target for HNSCC.

Keywords HNSCC, RBMS1, HSPA8, Proliferation, Migration and invasion, Therapeutic target

†Xinghong Yin and Meng Luo contributed equally to this work.

*Correspondence:
Maoli Duan
maoli.duan@ki.se
Yehai Liu
liuyehai@ahmu.edu.cn
[1] Department of Otorhinolaryngology Head & Neck Surgery, The First Affiliated Hospital of Anhui Medical University, No. 218 Jixi Road, Hefei, Anhui Province 230000, China
[2] Department of Otorhinolaryngology Head & Neck Surgery, Fuyang People's Hospital, Fuyang, China
[3] Department of Biochemistry & Molecular Biology, School of Basic Medicine, Anhui Medical University, Hefei, China
[4] Division of Ear, Nose and Thoat Disease, Department of Clinical Science, Intervention and Technology Karolinska Institutet, Stockholm, Sweden
[5] Ear Nose and Throat Patient Area, Trauma and Reconstructive Medicine, Karolinska University Hospital, Stockholm, Sweden

Introduction

Head and neck squamous cell carcinoma (HNSCC) ranks as the sixth most common cancer globally [1]. This malignancy originates from the squamous cells lining the mucosal surfaces of the head and neck and typically develops in sites such as the oral cavity, pharynx (including the nasopharynx, oropharynx, and hypopharynx), larynx, sinuses, nasal passages, and salivary glands. The concealed nature of these anatomical locations often leads to delayed diagnosis, with most cases identified only after the disease has progressed to advanced stages [2]. This delay presents a significant challenges for effective treatment. Current treatment options for HNSCC include surgery, radiation therapy, chemotherapy, targeted therapy, and immunotherapy [3]. Among the targeted and immunotherapeutic approaches, agents such as cetuximab-tyrosine kinase inhibitors targeting the epidermal growth factor receptor (EGFR) [4, 5], -and immune checkpoint inhibitors, such as anti-programmed cell death-1 (PD-1) antibodies (e.g., nivolumab [6] and pembrolizumab [4, 7]), have been approved for HNSCC treatment. Immune checkpoint inhibitors have improved the survival and therapeutic outcomes of some patients with HNSCC, thereby offering clinical benefits. However, despite these advancements, the prognosis of HNSCC patients remains suboptimal, underscoring the urgent need for new molecular targets and optimized clinical management strategies.

The RNA-binding protein RBMS1, initially discovered as MSSP-1 (Myc single-stranded DNA-binding protein 1), was first characterized for its ability to bind single-stranded DNA sequences within the c-Myc gene promoter region, thereby playing a role in the transcriptional repression of c-Myc target genes [8]. Studies have demonstrated that RBMS1 promotes tumor growth in glioblastoma by inhibiting ferroptosis—knockdown of RBMS1 suppresses cell proliferation, migration, and induces apoptosis, whereas the ferroptosis inhibitor Ferrostatin-1 partially reverses these effects [9]. Notably, RBMS1 exhibits tissue-specific duality: it suppresses metastasis in colon cancer by maintaining RNA stability [10], yet promotes ferroptosis evasion in lung cancer via eIF3d-mediated SLC7A11 translation [11], highlighting its context-dependent regulatory complexity. Beyond cancer, RBMS1 orchestrates critical biological processes through post-transcriptional regulation. During cellular senescence, RBMS1 stabilizes ANKRD1 mRNA, driving its elevated expression and contributing to the early stages of senescence [12]. During neurodevelopment, RBMS1 ensures the stability of Efr3a mRNA, a key regulator of neuronal progenitor migration and differentiation. Its depletion leads to delayed radial migration and impaired neuronal maturation [13]. Additionally, RBMS1 is highly expressed during the early phase of adipocyte differentiation, where it modulates metabolic gene networks, including carbohydrate and lipid metabolism. Its knockdown disrupts adipogenesis, thereby linking it to obesity and metabolic disorders [14]. Collectively, these findings highlighted RBMS1 as a versatile regulator of RNA stability in diverse biological contexts. The aforementioned studies have revealed that RBMS1 exhibits dual role in cancer, acting as both an oncogene and a tumor suppressor, which further piques our research interest. Through the analysis of public datasets, we initially identified that RBMS1 was significantly overexpressed in HNSCC, indicating its potential involvement in HNSCC progression.

However, the functional role of RBMS1 in HNSCC progression and its underlying molecular mechanisms remain largely unexplored. In the present study, we demonstrated that RBMS1 was significantly overexpressed in HNSCC and promoted the proliferation, migration, and invasion of HNSCC cells. Mechanistically, RBMS1 exerts oncogenic effects by upregulating HSPA8, a key regulator of protein homeostasis and cancer cell survival. These findings suggest that RBMS1 may serve as a promising therapeutic target for HNSCC and provide new insights into the molecular mechanisms driving HNSCC progression.

Materials and methods

Data and tumor specimen collection

Three HNSCC datasets-GSE127165, GSE37991, and GSE13601-were obtained from the GEO database (https://www.ncbi.nlm.nih.gov/geo/), whereas additional HNSCC datasets were sourced from TCGA database(http://www.cbioportal.org/). This dataset is expressed in transcripts per million (TPM) and normalized by $\log_2(TPM+1)$. The expression data of RBMS1 was extracted, and the gene expression data was divided into tumor tissue group and normal tissue group. This study included data from 20 cases of HNSCC and cancer-adjacent tissues from the Department of Otolaryngology-Head and Neck Surgery, The First Affiliated Hospital of Anhui Medical University, between 2020 and 2023. None of the patients received radiotherapy, chemotherapy, immunotherapy, or other anti-tumor treatments before surgery. This study followed the principles of the Declaration of Helsinki and was approved by the Research Ethics Committee of the First Affiliated Hospital of Anhui Medical University. Written informed consent was obtained from all patients prior to their participation.

Cell culture

FaDu and CAL27 cell lines were purchased from Ubigene (Guangzhou, China) and TU177 and NOK cell lines were obtained from Otwo Biotech (Guangzhou, China).

The above cell lines were cultured in RPMI-1640 (Gibco) or DMEM (Gibco) medium containing 10% fetal bovine serum (Lonsera) and incubated in a cell culture incubator at 37 °C with 5% CO_2. Cell cultures were frequently monitored for mycoplasma contamination, and only mycoplasma-negative cells were used in the experiments.

Western blot

Proteins were extracted from cells or tissues using RIPA lysis buffer, and their concentrations were determined using the BCA assay. Equal amounts of protein samples were mixed with 5×loading buffer at a 4:1 ratio and denatured by boiling for 5 min. The samples were separated by SDS-PAGE on NuPAGE 4–12% Bis–Tris gels and transferred onto PVDF membranes. To block non-specific binding, the membranes were incubated with 5% non-fat milk in 1×TBST for 1 h at room temperature. Subsequently, membranes were incubated with primary antibodies overnight at 4 °C, followed by incubation with HRP-conjugated secondary antibodies for 1 h at room temperature. Protein bands were visualized using enhanced chemiluminescence on a Tanon Imaging System. The following antibodies were used: Anti-beta actin (ab8226, Abcam, 1:10,000), Anti-GAPDH (ab8245, Abcam, 1:2,500), Anti-RBMS1 (11,061–2-AP, Proteintech, 1:2,000), Anti-HSPA8 (10654–1-AP, Proteintech, 1:1,000), Goat Anti-Rabbit IgG H&L (HRP) (ab6721, Abcam, 1:10,000), and Rabbit Anti-Mouse IgG H&L (HRP) (ab6728, Abcam, 1:10,000).

Lentivirus infection

Lentiviral vectors for gene knockdown and overexpression were constructed using Hanhen Bio software. Cells were cultured to 70–80% confluence before proceeding with the following steps: The lentiviral infection system was prepared and transfected according to the manufacturer's instructions. Cells transfected with an empty vector served as a control. Detailed information on the target sequences is provided in Supplementary Table S1. Lentiviral infection efficiency was confirmed using quantitative Real-time PCR (qRT-PCR) and western blotting to ensure that the target genes were successfully expressed or knocked down.

Immunohistochemistry (IHC)

Tumor tissues from each group were fixed in 4% paraformaldehyde for 12 h and embedded in paraffin blocks. The blocks were cut into 4 μm thick sections and stained with Anti-Ki67 antibody (ab15580, Abcam,1/200), Anti-RBMS1 antibody (MA5-27,025, ThermoFisher, 1:150 dilution), and Anti-HSPA8 (1:200 dilution).

qRT-PCR and RNA sequencing

RNA samples were extracted using the TRIzol method, reverse transcribed according to the instructions of the Revert Aid First Strand cDNA Synthesis Kit, and subjected to qPCR using the corresponding reagents to obtain accurate results. RNA samples were sequenced using Illumina NovaSeq 6000 (LC Sciences, Hangzhou, China). Differential gene expression analysis was performed using DESeq2, ensuring robust and accurate identification of differentially expressed genes between the experimental groups. The following primer sequences were used: human RBMS1 forward, 5′-AAGGTCACT AAGCAGCACAAT-3′, and reverse, 5′-CACGACTTG TACCACTGGAATCAC-3′; human HSPA8 forward, 5′-TGCTGTGGACAAGAGTACGG-3′, and reverse 5′-AGCTTCCTGGACCATACGTT-3′; EIF2AK2 forward, 5′- TCTTTTGCTACTACGTGTGAGT-3′, and reverse, 5′- CTGAGACCATTCATAAGCAACG-3′. EIF2AK3 forward, 5′- GCGTCGGAGACAGTGTTT GG-3′, and reverse, 5′- CGCAGTTCCACGTCGTCA TC-3′. HSPA5 forward, 5′- CAGTTGTTACTGTAC CAGCCTA-3′, and reverse, 5′- CATTTAGGCCAGCAA TAGTTCC-3′. XBP1 forward, 5′- CTTGTAGTTGAG AACCAGGAGT-3′, and reverse, 5′- CCCAACAGG ATATCAGACTCTG-3′. ATF3 forward, 5′- AACCTG ACGCCCTTTGTCAAG-3′, and reverse, 5′- TACCTC GGCTTTTGTGATGGA-3′. GAPDH forward, 5′-GGA GCGAGATCCCTCCAAAAT-3′, and reverse, 5′-GGC TGTTGTCATACTTCTCATGG-3′.

Cell proliferation assay

Logarithmically growing healthy cells were selected, washed thrice with PBS, and digested with trypsin before being resuspended in medium. Each experimental group was set up in triplicate in 96-well plates, with 100 μL of cell suspension containing 1,000 cells per well. The plates were incubated at 37 °C with 5% CO_2. On day 0, after allowing cells to adhere for at least 6 h, 100 μL of 10% CCK-8 solution was added to each well. After 2 h of incubation, the absorbance was measured at 450 nm using a microplate reader. The experiment was repeated at the same time points over four days, and the results are summarized accordingly.

Wound healing assay

Logarithmically growing, healthy cells were selected. The cells were then evenly distributed in 6-well plates and incubated overnight at 37 °C with 5% CO_2 until reaching 90% confluence. Using the tip of a 200 μL pipette, a narrow scratch was made vertically across the cell layer. The scratched area was photographed under a microscope to document the initial wound. The plates were then

incubated at 37 °C, 5% CO_2 for 24 h. After incubation, cell migration into the scratched area was observed and recorded under a microscope. Images of the scratched area were analyzed using ImageJ software to measure the healing area by comparing the scratched area before and after incubation.

Cell migration and invasion experiments

For migration experiments, the upper compartments of Transwell chambers were left uncoated, while for invasion experiments, the upper chambers were coated with 250 μg/mL Matrigel and incubated for 30–60 min to allow solidification. Cells were cultured in the appropriate medium until they reached the logarithmic growth phase, digested with trypsin, neutralized, and resuspended in the medium. After washing, cell concentration was adjusted to 2×10^4 cells per 200μL. In the upper chamber, 200μL of medium containing 1% FBS was added, while the lower chamber received 500μL of medium containing 10% FBS to promote cell migration. The transwell chambers were then placed in a 37 °C incubator with 5% CO_2 for 24–48 h, with minimal agitation.

At the end of the incubation period, the upper surface of the transwell filter was gently wiped with a sterile cotton swab to remove non-migrating or non-invasive cells. The filters were fixed in 4% paraformaldehyde for 10–15 min, washed with phosphate buffered saline (PBS), and stained for 15–20 min with crystal violet. After an additional wash with PBS, only the cells on the lower surface were stained. The cells on the lower surface of the filter were observed and counted under an inverted microscope at a magnification of 200x. Ten random fields of view were photographed, and the average cell count was recorded to quantify both the migration and invasion capacities.

Animal experiments

Four-week-old male BALB/c nude mice and NOD/SCID mice, aged 4 weeks, were purchased from GemPharmatech Co., Ltd. (Nanjing, China). Silenced or overexpressing cells were injected subcutaneously into each mouse. The health status of the mice was closely monitored throughout the study, including regular assessments of body weight, general condition, and signs of distress. Tumor growth was measured periodically, and tumor volumes were calculated using the formula: $V=0.5\times W^2\times L$ (where V represents volume, L represents length, and W represents width). Growth curves were plotted to track the tumor progression. At the end of the experiment, the mice were euthanized and tissues, including tumors, were collected for further analysis. The collected tissues were either fixed in formalin for histopathological examination or stored at -80 °C for molecular analysis. All animal procedures adhered to the ethical guidelines of the Institutional Animal Care and Use Committee (our). This study was approved by the Ethics Committee of Quick-PJ 2022–03-19. We ensured strict compliance with these guidelines to minimize animal suffering and ensure humane treatment throughout the study.

Statistical analysis

Data analysis was performed using GraphPad Prism (version 8.0 GraphPad Software San Diego(CA, USA). Differences between groups were evaluated using paired or unpaired t-tests or one-way ANOVA variance depending on the experimental design. The relationships between variables were examined using Pearson's correlation coefficient. Survival analysis was conducted using the Kaplan–Meier method. All experiments were repeated a minimum of three times, and a P-value of less than 0.05 was considered statistically significant.

Results

RBMS1 expression in four HNSCC datasets and validation in HNSCC tissue

To identify differentially expressed genes in head and neck squamous cell carcinoma (HNSCC), we analyzed three datasets- GSE127165, GSE37991, and GSE1301- from the GEO and TCGA databases to assess RBMS1 expression. The results demonstrated that RBMS1 expression was significantly higher in tumor tissues than in normal tissues, with all differences reaching statistical significance (Fig. 1A). In our study, we collected 20 fresh surgical specimens from patients with HNSCC, including 12 patients with laryngeal cancer, five patients with hypopharyngeal cancer, and three patients with tongue cancer. Western blot analysis confirmed that RBMS1 protein levels were significantly elevated in the tumor tissues (Fig. 1B). Similarly, qRT-PCR analysis of these specimens revealed that RBMS1 mRNA levels were higher in tumor tissues than in matched controls ($n=20$, ****, $p<0.0001$; Fig. 1C). Additionally, IHC was performed to investigate the expression and localization of RBMS1 in the HNSCC samples. The results indicated that RBMS1 was predominantly localized to the cytoplasm of tumor cells, further confirming its significantly elevated expression in cancer tissues (Fig. 1D).

RBMS1 promotes the HNSCC malignant phenotype

To further investigate the role of RBMS1 in the malignant behavior of HNSCC, including its proliferation, metastasis, and invasion, we conducted a series of experiments. We assessed RBMS1 mRNA and protein expression in three HNSCC cell lines (FaDu, CAL27, and TU177) using qRT-PCR and western blotting, with the NOK cell line serving as a control. The results demonstrated that

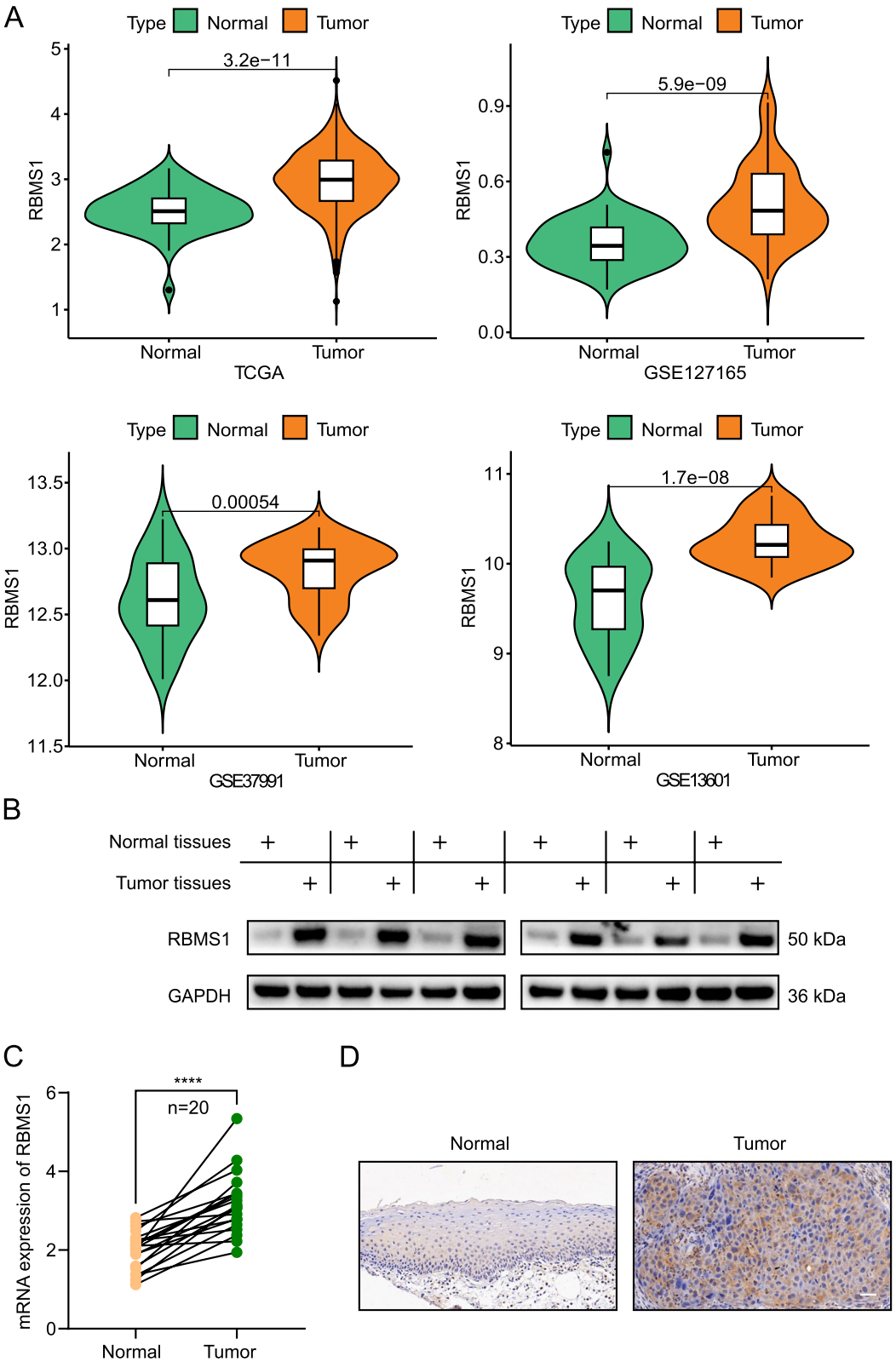

Fig. 1 RBMS1 expression in four HNSCC datasets and validation in HNSCC tissue. **A** Expression of RBMS1 in TCGA-HNSCC, GSE127165, GSE37991, and GSE13601 databases. **B** Western blot detection of RBMS1 protein expression in tissues (representative image); **C** qRT-PCR analysis of RBMS1 mRNA expression in 20 paired HNSCC samples ($n = 20$, ****, $p < 0.0001$); **D** IHC staining to detect the expression and localization of RBMS1 in HNSCC specimens. Scale = 40 μm

RBMS1 expression levels were the highest in FaDu cells, followed by CAL27 and TU177 cells (Fig. 2A-B). Based on these findings, we selected TU177 and FaDu cells to construct stable knockdown and overexpression models, respectively. RBMS1 knockdown and overexpression were confirmed by western through WB and qRT-PCR, respectively (Fig. 2C-D).

To elucidate the effect of RBMS1 knockdown on TU177 cell characteristics, a CCK-8 assay was performed, and the results showed that RBMS1 knockdown significantly reduced TU177 cell proliferation compared to control cells(Fig. 2E). Colony formation assays confirmed this, showing fewer colonies following RBMS1 knockdown, highlighting its role in cell proliferation (Fig. 2G). Wound healing and transwell migration/invasion assays further demonstrated that RBMS1 knockdown significantly impaired TU177 cell migration and invasion (Fig. 2I and K). Overexpression of RBMS1 in FaDu cells significantly enhanced cell proliferation and colony formation, as demonstrated by the CCK-8 and colony formation assays (Fig. 2F and H). Furthermore, RBMS1-overexpressing FaDu cells exhibited increased migration in scratch assays and significantly promoted cell migration and invasion in Transwell assays (Fig. 2J and L). These findings indicated that RBMS1 overexpression markedly boosted the proliferative, migratory, and invasive capabilities of FaDu cells.

RBMS1 promotes HNSCC tumor growth in vivo

Previous studies have shown that RBMS1 promoted HNSCC cell proliferation in vitro. To further investigate its role in vivo, we assessed the effect of RBMS1 knockdown and overexpression on tumor growth in a mouse xenograft model. TU177 control cells and RBMS1 knockdown cells were injected subcutaneously into the flanks of nude mice. The reduced expression of RBMS1 significantly diminished the tumorigenic potential of TU177 cells compared to that of control cells (Fig. 3A-C). Subsequently, we injected FaDu control cells and cells overexpressing RBMS1 into immunodeficient mice. The results demonstrated that tumors in the LvRBMS1 group were larger and heavier than those in the control group (Fig. 3E-G). IHC analysis further revealed that Ki-67 staining, a crucial marker of cell proliferation, was markedly reduced in tumors with RBMS1 knockdown, whereas the staining intensity was significantly increased in tumors with RBMS1 overexpression (Fig. 3D and H). Collectively, these findings highlight the critical role of RBMS1 in enhancing HNSCC cell proliferation in vivo.

HSPA8 serves as a downstream target of RBMS1

To further explore the downstream regulatory network of RBMS1, we performed a comparative analysis of gene expression profiles between RBMS1 knockdown cells (shRBMS1) and control (shSc) TU177 cells using RNA sequencing. This analysis identified a total of 1,314 significantly differentially expressed genes (DEGs) in RBMS1 knockdown cells relative to the controls, comprising 524 upregulated and 790 downregulated genes ($|Log_2FC| > 1$, $p < 0.05$) (Fig. 4A and Fig. S1A). GO analysis revealed that the knockdown of RBMS1 significantly affected various crucial biological processes, notably the cellular response to external stimuli, response to unfolded proteins, and small GTPase-mediated signal transduction(Fig. 4B). Furthermore, the enrichment of cellular components and molecular functions underscored the extensive impact of RBMS1 on microtubule and GTPase regulatory activities (Fig. 4C-D). KEGG analysis revealed several significant biological pathways impacted by RBMS1 knockdown, including the PI3K – Akt signaling pathway, Rap1, p53, and MAPK signaling pathways (Fig. S1B). Collectively, the results from both GO and KEGG analyses highlighted the regulatory function of RBMS1 in cellular processes and stress responses, indicating its potential impact on tumor cell proliferation and survival via various tumor-associated signaling pathways.

To further elucidate the candidate genes linked to the downstream effects of RBMS1, we categorized biological processes using GO analysis. A comparative analysis was conducted between genes in the subclass 'cellular response to external stimulus' and those in the 'response to unfolded protein' subclass. Six shared genes were identified: HSPA8, EIF2AK2, EIF2AK, HSPA5, XBP1, and ATF3. HSPA8 showed the most pronounced differential expression. We further validated these results using qRT-PCR (Fig. 4E and Fig. S1C-G). In TU177 cells, silencing of

(See figure on next page.)

Fig. 2 Effects of RBMS1 Knockdown and Overexpression on HNSCC Cell Phenotypes. **A**-**B** qRT-PCR and Western blot analysis of RBMS1 expression in NOK and three HNSCC cell lines. **C**-**D** Western blot and qRT-PCR validation of RBMS1 knockdown and overexpression efficiency in TU177 and FaDu cells (****$p < 0.0001$). **E**–**H** CCK-8 and colony formation assays demonstrate that RBMS1 knockdown in TU177 cells reduces proliferation and colony formation, while RBMS1 overexpression in FaDu cells enhances these phenotypes compared to controls (shsc or Lv). **I**-**J** Wound healing assays show that RBMS1 knockdown in TU177 cells slows migration, whereas RBMS1 overexpression in FaDu cells accelerates wound closure. **K**-**L** Transwell assays reveal that RBMS1 knockdown in TU177 cells reduces migration and invasion, while RBMS1 overexpression in FaDu cells significantly enhances these capabilities

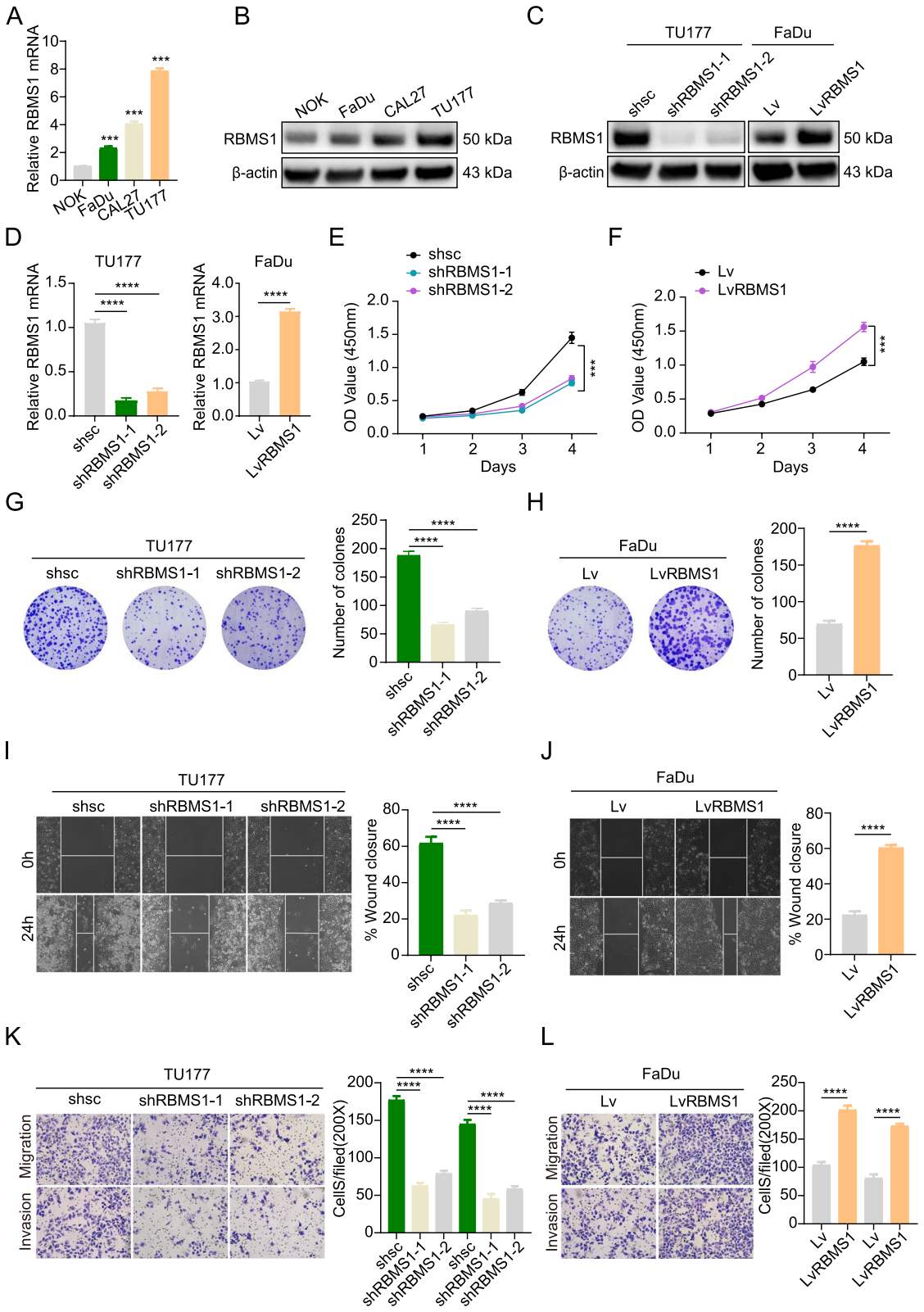

Fig. 2 (See legend on previous page.)

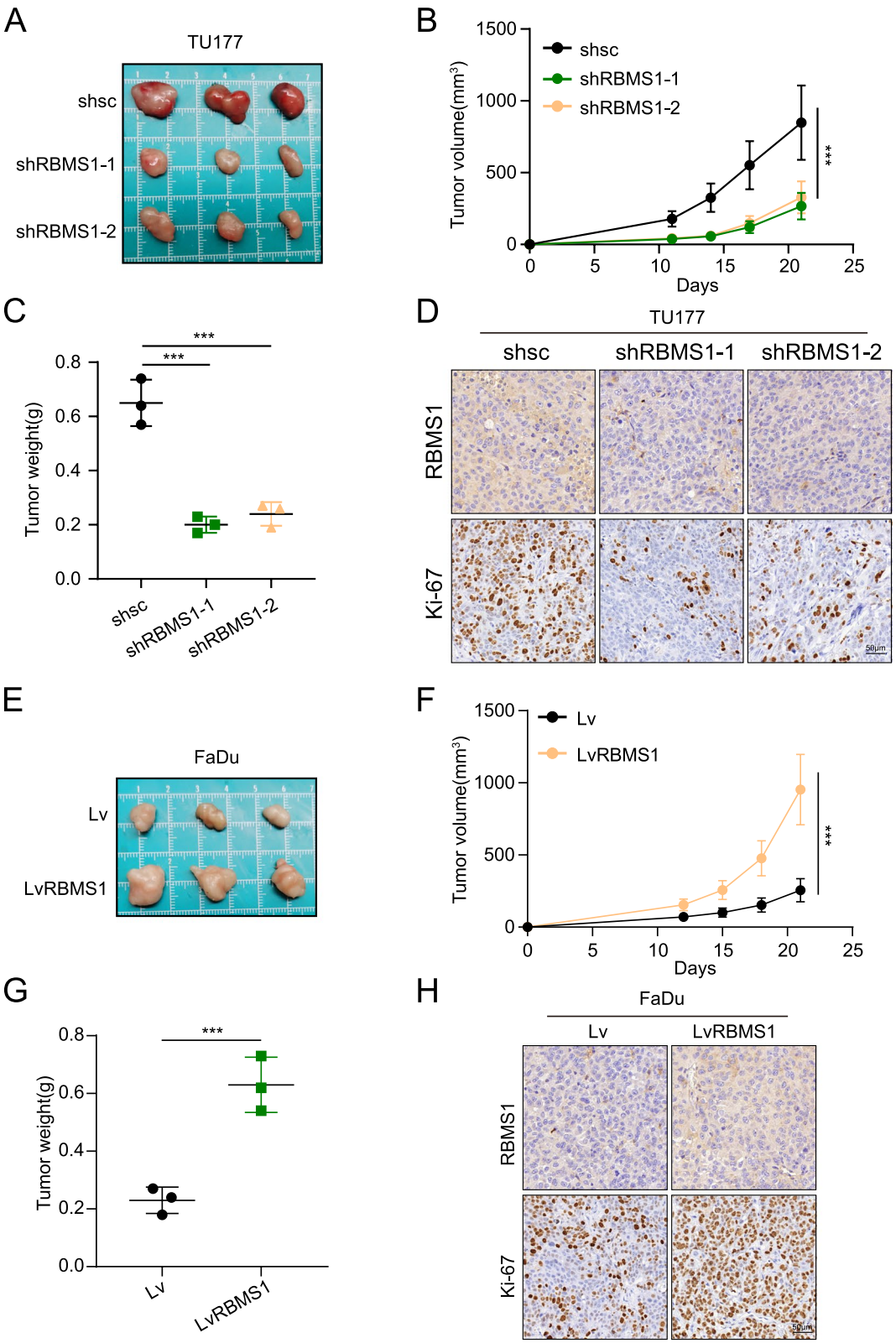

Fig. 3 RBMS1 promotes HNSCC tumor growth in vivo. Cells were subcutaneously injected into nude mice, and tumor growth was monitored. Tumor images (**A**, **E**), volume at specified time points (**B**, **F**), weight (**C**, **G**), and representative IHC staining of RBMS1 and Ki-67 are shown (**D**, **H**). Error bars represent the mean ± standard deviation (n = 3 per group). Scale bar = 50 μm

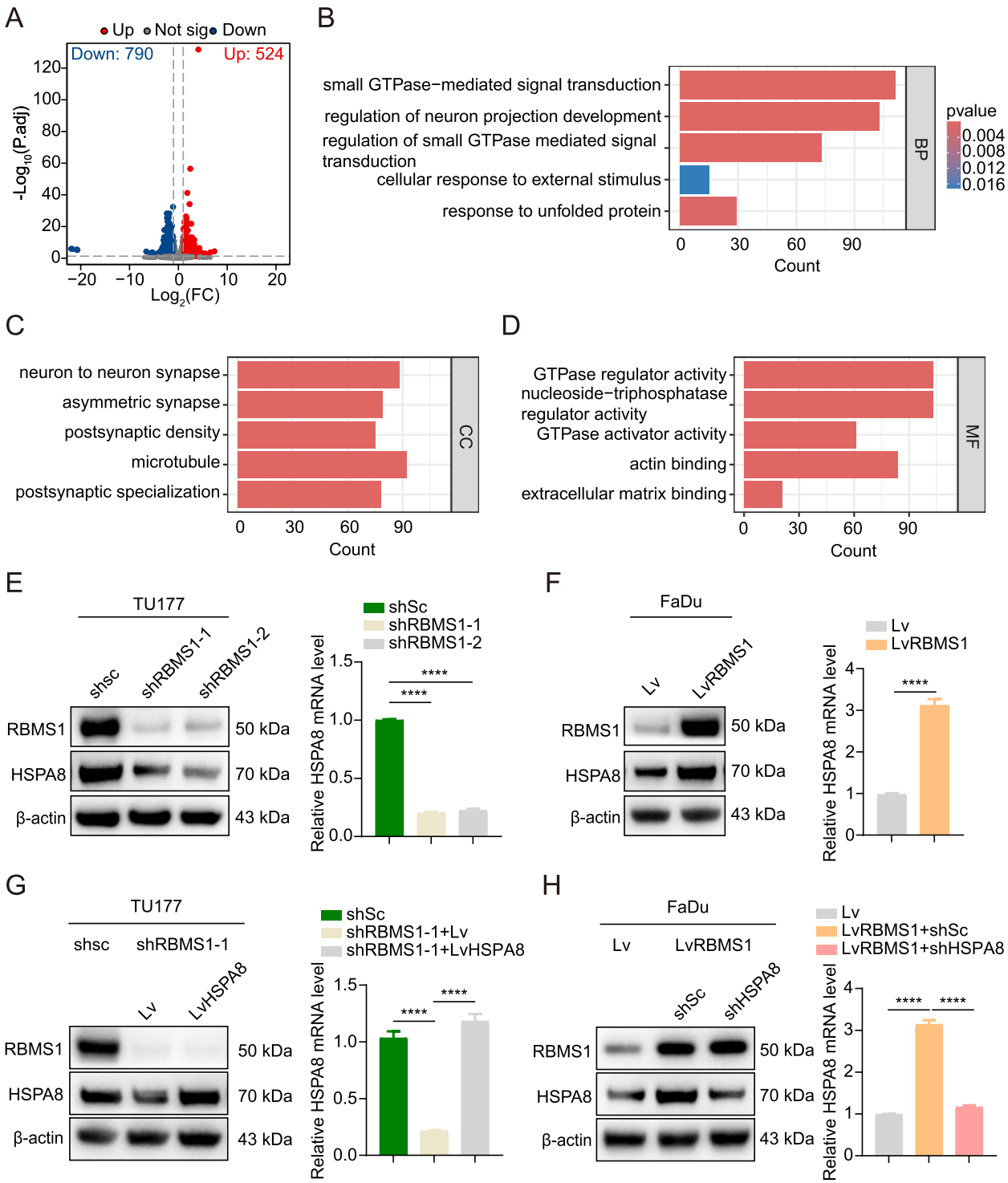

Fig. 4 RBMS1 regulates HSPA8 expression. **A** Display 1314 differential genes using volcano map. **B**-**D** GO analysis of differentially expressed genes. **E** shRBMS1 and shSc TU177 cells. **F** RBMS1-overexpressing FaDu and the control cells. **E**–**F** HSPA8 levels were examined by Western blot (left panels) and qRT-PCR (right panels). **G** shRBMS1 TU177 cells were infected with lentiviruses carrying an empty vector (vector) or expression vectors for HSPA8. **H** RBMS1-overexpressing FaDu cells were infected with lentivirus harboring HSPA8 shRNA or a scrambled shRNA (shSc). RBMS1, HSPA8 protein and mRNA levels were examined by Western blot and qRT-PCR

RBMS1 (using shRBMS1-1 and shRBMS1-2) significantly reduced HSPA8 levels (Fig. 4E). Conversely, RBMS1 overexpression in FaDu cells markedly increased HSPA8 expression (Fig. 4F). Rescue experiments demonstrated that HSPA8 overexpression partially restored HSPA8 levels in RBMS1-knockdown TU177 cells (Fig. 4G), whereas HSPA8 knockdown in RBMS1-overexpressing FaDu cells decreased HSPA8 expression (Fig. 4H). Collectively, these findings confirm that HSPA8 is a downstream target of RBMS1 and plays a critical role in mediating its oncogenic effects.

RBMS1 promotes proliferation, and metastasis of HNSCC cells through upregulation of HSPA8.

The role of HSPA8 in mediating the proliferative function of RBMS1 was evaluated in a series of experiments. In the TU177 cell line, experimental findings demonstrate that HSPA8 plays a pivotal role in RBMS1-mediated regulation of cell proliferation. As shown in Fig. 5A, the results of the CCK-8 assay indicated that HSPA8 overexpression partially rescued the reduced proliferative capacity caused by the RBMS1 knockdown. Colony formation assays further corroborated these findings, with HSPA8 overexpression restoring colony numbers in RBMS1-knockdown cells (Fig. 5B-C). In the wound healing assay (Fig. 5G-H), HSPA8 overexpression effectively counteracted the suppression of cell migration induced by RBMS1 knockdown. Furthermore, Transwell assays demonstrated that RBMS1 knockdown significantly inhibited the migratory and invasive abilities of TU177 cells, while these effects were partially restored upon HSPA8 overexpression (Fig. 5K-L). HSPA8 knockdown antagonizes the effects of RBMS1 overexpression in FaDu cells As illustrated in Fig. 5D, CCK-8 assay showed that HSPA8 knockdown markedly reduced the proliferation-promoting effects of RBMS1 overexpression. Colony formation assays confirmed these results, showing a reduction in colony number upon HSPA8 knockdown in RBMS1-overexpressing cells (Fig. 5E-F). Similarly, wound healing assays demonstrated that HSPA8 knockdown mitigated RBMS1-induced migration enhancement in FaDu cells (Fig. 5I-J). In addition, transwell assays confirmed that HSPA8 knockdown significantly suppressed the RBMS1 overexpression-mediated increase in migration and invasion abilities (Fig. 5M-N). These results clearly demonstrate that HSPA8 plays a crucial role in the regulation of the proliferation, migration, and invasion of HNSCC cells through RBMS1.

RBMS1 promotes through upregulation of HSPA8 tumor growth

In a CDX model constructed using TU177 cells, HSPA8 overexpression partially counteracted the inhibitory effect of RBMS1 knockdown on tumor growth. Specifically, tumor volume and weight were significantly increased in the HSPA8 overexpression group (Fig. 6A-C). IHC analysis further demonstrated that HSPA8 overexpression partially restored the proliferative capacity of tumor cells, a result further supported by a significant increase in the number of Ki-67-positive cells (Fig. 6D). The tumor volume and weight in the group injected with LvRBMS1 cells with HSPA8 knockdown were significantly lower than those in the control group injected with LvRBMS1 cells alone (Fig. 6E-G). Specifically, compared to the LvRBMS1 group, the tumor volume was markedly reduced, and the tumor weight was significantly decreased in the LvRBMS1 cells with HSPA8 knockdown. Similar results were observed with Ki-67 staining (Fig. 6H).

Discussion

The incidence and mortality rates of HNSCC have been rising annually [1, 15]. Existing targeted therapies show limited efficacy, particularly in advanced and recurrent cases, highlighting the urgent need for new therapeutic targets to improve patient prognosis and treatment outcomes. Our pan-cancer multi-omics analysis of RBMS1 revealed its differential expression across various cancer types, suggesting its potential diagnostic and prognostic significance in most malignancies.

Numerous studies have been conducted on RBMS1 in the past. For example, in non-small cell lung cancer, RBMS1 drives metastasis via YTHDF1-mediated translation of S100P, a process that can be targeted by the small-molecule inhibitor NTP [16]. In colorectal cancer, RBMS1 confers oxaliplatin resistance by inducing prion protein-mediated ferroptosis evasion, and its inhibition restores chemosensitivity [17]. Similarly, the circIDE/miR-19b-3p/RBMS1 axis regulates ferroptosis in hepatocellular carcinoma, and low RBMS1 expression serves as

(See figure on next page.)

Fig. 5 HSPA8 is a functionally important downstream target of RBMS1 in HNSCC cells. **A**-**C**, **G**-**H**, **K**-**L**. shRBMS1-1 TU177 cells were infected with lentiviruses carrying an empty vector or expression vectors for HSPA8. **D**-**F**, **I**-**J**, **M**–**N** RBMS1-overexpressing FaDu cells were infected with lentivirus harboring HSPA8 shRNAs or a scrambled shRNA. The cell proliferation and migratory abilities of the indicated cells were evaluated by CCK-8 (**A** and **D**), colony formation assays (**B**-**C** and **E**–**F**), and wound healing assays (**G**-**H** and **I**-**J**). **K**-**L** and **M**–**N** Cell migration and invasion abilities of the indicated cells were measured by transwell assays

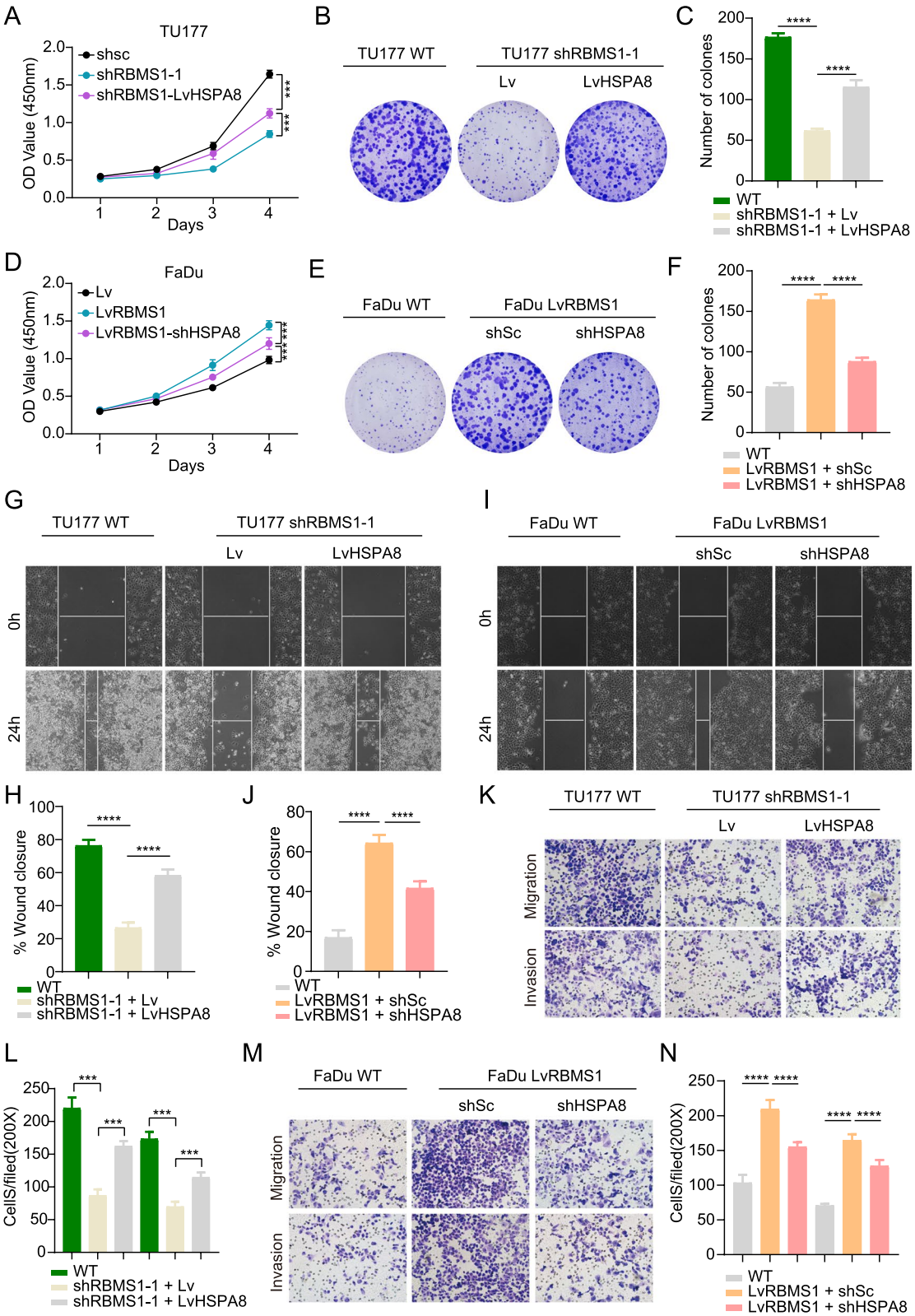

Fig. 5 (See legend on previous page.)

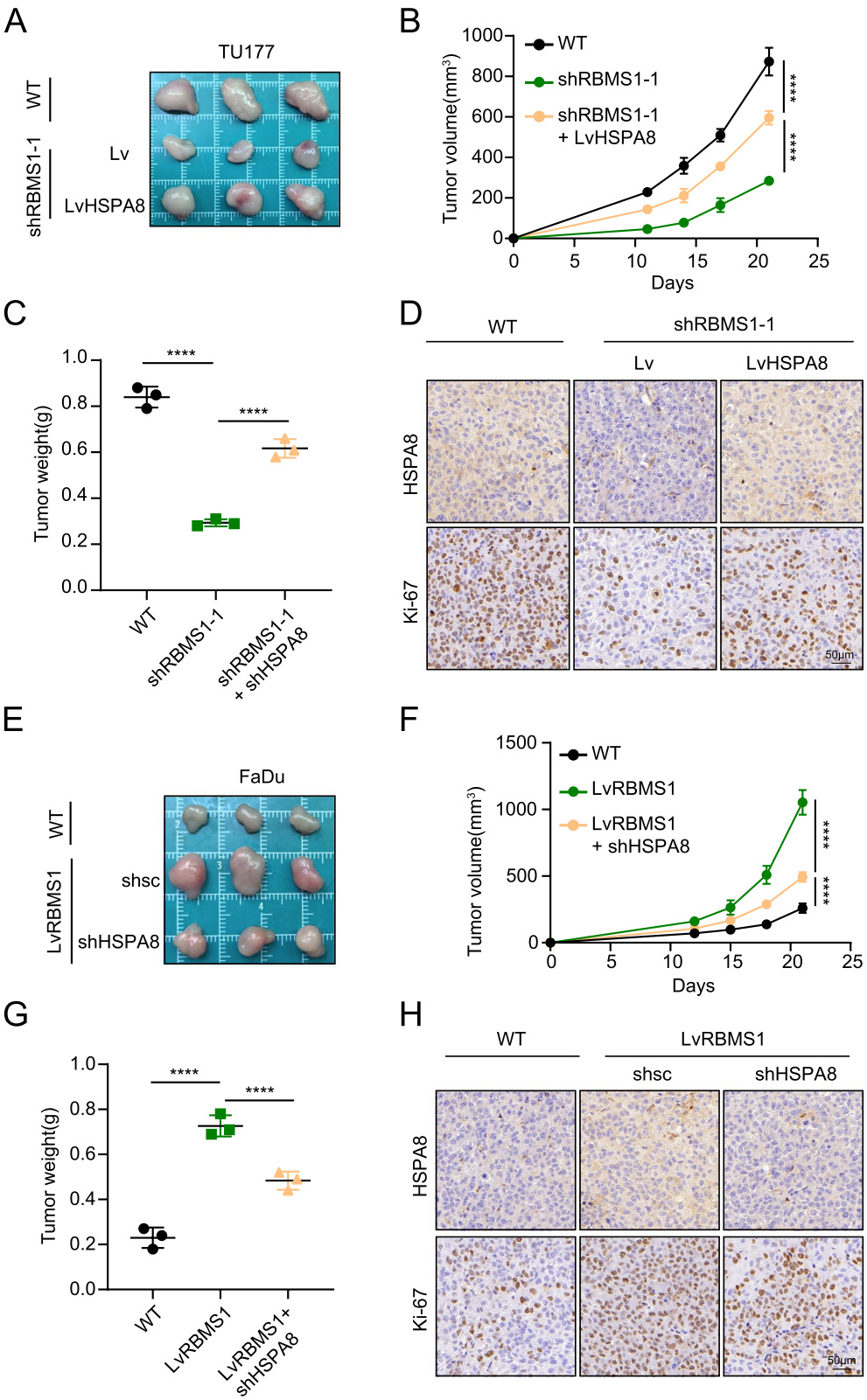

Fig. 6 RBMS1 promotes tumor growth through HSPA8 upregulation. Tumor growth of mice subcutaneously inoculated with the indicated cells. $N = 3$ for each group. **A** and **E** Tumor pictures. **B** and **F** Tumor growth curves. **C** and **G** Tumor weight. **D** and **H** Representative IHC staining for HSPA8 and Ki-67 of the indicated tumor tissues

a predictor of poor prognosis [18]. Additionally, RBMS1 promotes metastasis in gastric cancer by activating the IL-6/JAK2/STAT3 pathway, and its overexpression is strongly correlated with unfavorable clinical outcomes [19]. RBMS1, which acts as a tumor suppressor, is targeted by the oncogenic miR-106b in prostate cancer, and its loss accelerates tumor proliferation and migration [20]. In triple-negative breast cancer, RBMS1 stabilizes B4GALT1 mRNA to regulate PD-L1 glycosylation, and its depletion enhances the efficacy of the CTLA4 checkpoint blockade [21].

In this study, we analyzed datasets from GSE127165, GSE37991, and GSE1301 in conjunction with data from TCGA and discovered that RBMS1 expression was markedly increased in HNSCC tumor tissues compared to normal tissues. We obtained samples from 20 patients with HNSCC and used western blotting, qRT-PCR, and IHC to verify the elevated expression of RBMS1 in tumor specimens. To gain further insight into RBMS1's role in HNSCC biology, we manipulated RBMS1 expression in TU177 cells through knockdown, and in FaDu cells via overexpression, mirroring the diverse RBMS1 levels observed across different cell lines.

Our in vitro and in vivo experiments confirmed that RBMS1 exerts a significant tumor-promoting effect on HNSCC. Specifically, the overexpression of RBMS1 markedly enhances the proliferation, migration, and invasion of HNSCC cells, whereas the knockdown of RBMS1 suppresses these aggressive phenotypes. In vivo studies corroborated these findings, revealing that RBMS1 overexpression accelerated tumor growth, whereas RBMS1 knockdown significantly reduced tumor volume and weight.

To explore the underlying mechanisms the of RBMS1 action, RNA sequencing was conducted on TU177 cells with RBMS1 knockdown (shRBMS1) and a control (shSc). Based on GO analysis, we identified HSPA8 as a potential downstream target of RBMS1. HSPA8, a member of the heat shock protein family, plays crucial roles in protein homeostasis, folding, degradation, and autophagy [22]. Existing literature suggests that HSPA8 contributes to tumorigenesis in various cancers [23]. For instance, BAG-1, which interacts with HSPA8, enhances cell migration in gastric cancer [24]. HSPA8 is also vital in chaperone-mediated autophagy, facilitating the transport of proteins to lysosomes and influencing cancer cell proliferation while reducing drug sensitivity [25, 26]. In glioblastomas, nestin regulates stemness, growth, and invasion by modulating HSPA8 expression, suggesting that targeting these pathways may offer therapeutic benefits [27]. HSPA8 is upregulated in BRAF V600E colorectal cancer, where it promotes tumor progression by degrading CAV1 to release β-catenin and activate the Wnt/β-catenin pathway, and the HSPA8 inhibitor VER155008 exhibits synergistic effects with BRAF inhibitors, suggesting that HSPA8 could serve as a therapeutic target for refractory BRAF V600E CRC [28]. HSPA8 acts as a negative feedback regulator in diabetic kidney disease by regulating INSIG1/2 phosphorylation, disrupting the interaction between INSIG and SCAP and promoting PKR degradation to inhibit lipogenesis in renal tubular epithelial cells. Under high-glucose stimulation, SREBP1 upregulates HSPA8 expression, whereas persistently high glucose suppresses HSPA8 expression via NF-κB, promoting the progression of diabetic kidney disease [29]. Previous studies have shown that HSPA8 knockdown reduces spinal cord ischemia–reperfusion injury and promotes motor function recovery by inhibiting astrocyte activation and related inflammatory responses, thus providing a potential therapeutic strategy [30]. Other studies have shown that the downregulation of HSPA8 promotes the degradation of the E3 ubiquitin ligase SKP2, which attenuates the ubiquitination of NLRP3, activates the NLRP3 inflammasome, and mediates pyroptosis in alveolar epithelial cells, thus providing a new therapeutic target for the treatment of sepsis-induced acute lung injury [31]. As suggested by the study, HSPA8, in conjunction with ALDH2, regulates fibroblast senescence following oxygen–glucose deprivation (OGD), offering a novel direction and foundation for effectively intervening in fibroblast senescence after myocardial infarction [32].

Given the above research on HSPA8, it is reasonable to choose HSPA8 as a potential downstream target of RBMS1.Our Western blot experiments demonstrated that RBMS1 knockdown reduced HSPA8 expression, whereas RBMS1 overexpression increased it, confirming HSPA8's status as a downstream target. Rescue experiments showed that HSPA8 overexpression partially restored HSPA8 levels in RBMS1-knockdown TU177 cells, whereas HSPA8 knockdown diminished the HSPA8 expression induced by RBMS1 overexpression in FaDu cells. Further in vitro assays, including CCK-8, colony formation, scratch, and Transwell assays, corroborated that HSPA8 mediates the effects of RBMS1 on HNSCC cell proliferation, migration, and invasion. In vivo experiments demonstrated that HSPA8 overexpression partially mitigated tumor growth inhibition resulting from RBMS1 knockdown, whereas HSPA8 knockdown suppressed the tumor-promoting effects of RBMS1 overexpression. These findings are consistent with those of previous studies, highlighting the role of HSPA8 in tumor progression and reinforcing the notion that RBMS1 regulates HNSCC proliferation, migration, and invasion through HSPA8.

Although our study revealed the tumor-promoting role of RBMS1 in HNSCC and the molecular

mechanisms mediated by HSPA8, many unanswered questions and potential research directions remain to be explored. First, how RBMS1 precisely regulates HSPA8 expression and its downstream signaling pathways require further investigation. Co-immunoprecipitation experiments demonstrated a direct interaction between RBMS1 and HSPA8 at the protein level. This finding suggests that RBMS1 not only regulates HSPA8 expression at the transcriptional level, but may also modulate HSPA8 function at the post-translational level through protein–protein interactions. These multilayered regulatory mechanisms may enable RBMS1 to finely tune HSPA8 activity, thereby influencing the malignant phenotype of HNSCC. Second, the therapeutic potential of RBMS1 warrants further investigation. Based on our findings, high RBMS1 expression in HNSCC was closely associated with tumor proliferation, migration, and invasion. Therefore, the developing of RBMS1-targeted inhibitors or gene therapies may provide new treatment options for patients with HNSCC. Future studies should explore the application of small-molecule inhibitors, RNA interference techniques, or CRISPR/Cas9 gene editing to target RBMS1 and evaluate their efficacy and safety in preclinical models. Clinical translational research is a key direction for future studies. Although our study provided foundational experimental evidence for the role of RBMS1 in HNSCC, its feasibility and effectiveness in clinical applications require validation in large-scale clinical studies. Future research should investigate the potential of RBMS1 as a biomarker for HNSCC and evaluate its applicability in personalized treatment strategies.

Conclusion

In conclusion, RBMS1 plays a crucial role in promoting the proliferation, metastasis, and invasion of HNSCC cells. These findings highlight the promising application of RBMS1 as a therapeutic target for HNSCC.

Supplementary Information

The online version contains supplementary material available at https://doi.org/10.1186/s12885-025-13937-z.

Supplementary Material 1.
Supplementary Material 2.
Supplementary Material 3.
Supplementary Material 4.
Supplementary Material 5.

Acknowledgements
We would like to express our sincere gratitude to the publicly available TCGA, GEO, and ICGC databases for their invaluable resources.

Authors' contributions
Xinghong Yin: Writing—original draft, conceptualization, software. Meng Luo: Writing—review and editing, experimental completion. Xiaojun Zha review and editing (supporting). Maoli Duan formal analysis (supporting); methodology (supporting) Yehai Liu: Supervision, methodology, funding acquisition. All authors contributed to this manuscript and approved the final version.

Funding
This work was supported by the Natural Science Foundation of China (82171127, 82371133, 82171128 and 82303021), Anhui Provincial Natural Science Foundation (2208085MH239), the Natural Science Foundation of Universities of Anhui Province (2022AH051134) and Discipline Construction Project of the First Affiliated Hospital of Anhui Medical University (NO. 4245).

Data availability
In this study, bioinformatics data were sourced from the following publicly accessible databases: The Cancer Genome Atlas (TCGA): https://portal.gdc.cancer.gov/, International Cancer Genome Consortium (ICGC): https://dcc.icgc.org/, Gene Expression Omnibus (GEO): https://www.ncbi.nlm.nih.gov/geo/. These open-access resources provided comprehensive genomic and clinical data essential for our analyses.

Declarations

Ethics approval and consent to participate
This research involving human participants was reviewed and approved by the Ethics Committee of the First Affiliated Hospital of Anhui Medical University (Quick-PJ 2021–02-32). Written informed consent was obtained from all patients prior to their participation in this study.
Animal experiments were conducted following approval from the Institutional Animal Care and Use Committee (IACUC) of the First Affiliated Hospital of Anhui Medical University (Approval Number: Quick-PJ 2022–03-19). All procedures adhered to the ethical guidelines for animal research.

Consent for publication
Not applicable.

Competing interests
The authors declare no competing interests.

Received: 18 November 2024 Accepted: 13 March 2025
Published online: 27 March 2025

References

1. Sung H, Ferlay J, Siegel RL, Laversanne M, Soerjomataram I, Jemal A, Bray F. Global Cancer Statistics 2020: GLOBOCAN Estimates of Incidence and Mortality Worldwide for 36 Cancers in 185 Countries. CA Cancer J Clin. 2021;71(3):209–49.
2. Johnson DE, Burtness B, Leemans CR, Lui VWY, Bauman JE, Grandis JR. Head and neck squamous cell carcinoma. Nat Rev Dis Primers. 2020;6(1):92.
3. Maghami E, Ismaila N, Alvarez A, Chernock R, Duvvuri U, Geiger J, Gross N, Haughey B, Paul D, Rodriguez C, et al. Diagnosis and Management of Squamous Cell Carcinoma of Unknown Primary in the Head and Neck: ASCO Guideline. J Clin Oncol. 2020;38(22):2570–96.
4. Burtness B, Harrington KJ, Greil R, Soulières D, Tahara M, de Castro G, Jr., Psyrri A, Basté N, Neupane P, Bratland Å et al. Pembrolizumab alone or with chemotherapy versus cetuximab with chemotherapy for recurrent or metastatic squamous cell carcinoma of the head and neck (KEYNOTE-048): a randomised, open-label, phase 3 study. Lancet (London, England). 2019;394(10212):1915-1928.
5. Vermorken JB, Mesia R, Rivera F, Remenar E, Kawecki A, Rottey S, Erfan J, Zabolotnyy D, Kienzer HR, Cupissol D, et al. Platinum-based chemotherapy plus cetuximab in head and neck cancer. N Engl J Med. 2008;359(11):1116–27.
6. Ferris RL, Blumenschein G Jr, Fayette J, Guigay J, Colevas AD, Licitra L, Harrington K, Kasper S, Vokes EE, Even C, et al. Nivolumab for Recurrent

Squamous-Cell Carcinoma of the Head and Neck. N Engl J Med. 2016;375(19):1856–67.
7. Harrington KJ, Burtness B, Greil R, Soulières D, Tahara M, de Castro G, Jr., Psyrri A, Brana I, Basté N, Neupane P, et al. Pembrolizumab With or Without Chemotherapy in Recurrent or Metastatic Head and Neck Squamous Cell Carcinoma: Updated Results of the Phase III KEYNOTE-048 Study. J Clin Oncol. 2023;41(4):790–802.
8. Kimura K, Saga H, Hayashi K, Obata H, Chimori Y, Ariga H, Sobue K. c-Myc gene single-strand binding protein-1, MSSP-1, suppresses transcription of alpha-smooth muscle actin gene in chicken visceral smooth muscle cells. Nucleic Acids Res. 1998;26(10):2420–5.
9. Liang X, Wang G, Xue C, Zhou Y. RBMS1 interference inhibits malignant progression of glioblastoma cells and promotes ferroptosis. Discover Oncol. 2024;15(1):548.
10. Yu J, Navickas A, Asgharian H, Culbertson B, Fish L, Garcia K, Olegario JP, Dermit M, Dodel M, Hänisch B, et al. RBMS1 Suppresses Colon Cancer Metastasis through Targeted Stabilization of Its mRNA Regulon. Cancer Discov. 2020;10(9):1410–23.
11. Zhang W, Sun Y, Bai L, Zhi L, Yang Y, Zhao Q, Chen C, Qi Y, Gao W, He W, et al. RBMS1 regulates lung cancer ferroptosis through translational control of SLC7A11. J Clin Investig. 2021;131(22):e152067.
12. Shin CH, Rossi M, Anerillas C, Martindale JL, Yang X, Ji E, Pal A, Munk R, Yang JH, Tsitsipatis D, et al. Increased ANKRD1 Levels in Early Senescence Mediated by RBMS1-Elicited ANKRD1 mRNA Stabilization. Mol Cell Biol. 2024;44(5):194–208.
13. Habib K, Bishayee K, Kang J, Sadra A, Huh SO. RNA Binding Protein Rbms1 Enables Neuronal Differentiation and Radial Migration during Neocortical Development by Binding and Stabilizing the RNA Message for Efr3a. Mol Cells. 2022;45(8):588–602.
14. Dairi G, Al Mahri S, Benabdelkamel H, Alfadda AA, Alswaji AA, Rashid M, Malik SS, Iqbal J, Ali R, Al Ibrahim M, et al. Transcriptomic and Proteomic Analysis Reveals the Potential Role of RBMS1 in Adipogenesis and Adipocyte Metabolism. Int J Mol Sci. 2023;24(14):11300.
15. Bray F, Ferlay J, Soerjomataram I, Siegel RL, Torre LA, Jemal A. Global cancer statistics 2018: GLOBOCAN estimates of incidence and mortality worldwide for 36 cancers in 185 countries. CA Cancer J Clin. 2018;68(6):394–424.
16. Sun Y, Chen D, Sun S, Ren M, Zhou L, Chen C, Zhao J, Wei H, Zhao Q, Qi Y et al. RBMS1 Coordinates with the m(6)A Reader YTHDF1 to Promote NSCLC Metastasis through Stimulating S100P Translation. Adv Sci (Weinheim, Baden-Wurttemberg, Germany). 2024;11(15):e2307122.
17. Xu Y, Hao J, Chen Q, Qin Y, Qin H, Ren S, Sun C, Zhu Y, Shao B, Zhang J, et al. Inhibition of the RBMS1/PRNP axis improves ferroptosis resistance-mediated oxaliplatin chemoresistance in colorectal cancer. Mol Carcinog. 2024;63(2):224–37.
18. Zhai H, Zhong S, Wu R, Mo Z, Zheng S, Xue J, Meng H, Liu M, Chen X, Zhang G, et al. Suppressing circIDE/miR-19b-3p/RBMS1 axis exhibits promoting-tumour activity through upregulating GPX4 to diminish ferroptosis in hepatocellular carcinoma. Epigenetics. 2023;18(1):2192438.
19. Liu M, Li H, Zhang H, Zhou H, Jiao T, Feng M, Na F, Sun M, Zhao M, Xue L, et al. RBMS1 promotes gastric cancer metastasis through autocrine IL-6/JAK2/STAT3 signaling. Cell Death Dis. 2022;13(3):287.
20. Dankert JT, Wiesehöfer M, Wach S, Czyrnik ED, Wennemuth G. Loss of RBMS1 as a regulatory target of miR-106b influences cell growth, gap closing and colony forming in prostate carcinoma. Sci Rep. 2020;10(1):18022.
21. Zhang J, Zhang G, Zhang W, Bai L, Wang L, Li T, Yan L, Xu Y, Chen D, Gao W, et al. Loss of RBMS1 promotes anti-tumor immunity through enabling PD-L1 checkpoint blockade in triple-negative breast cancer. Cell Death Differ. 2022;29(11):2247–61.
22. Stricher F, Macri C, Ruff M, Muller S. HSPA8/HSC70 chaperone protein: structure, function, and chemical targeting. Autophagy. 2013;9(12):1937–54.
23. Albakova Z, Armeev GA, Kanevskiy LM, Kovalenko EI, Sapozhnikov AM. HSP70 Multi-Functionality in Cancer. Cells. 2020;9(3):587.
24. Naishiro Y, Adachi M, Okuda H, Yawata A, Mitaka T, Takayama S, Reed JC, Hinoda Y, Imai K. BAG-1 accelerates cell motility of human gastric cancer cells. Oncogene. 1999;18(21):3244–51.
25. Yang F, Xie HY, Yang LF, Zhang L, Zhang FL, Liu HY, Li DQ, Shao ZM. Stabilization of MORC2 by estrogen and antiestrogens through GPER1- PRKACA-CMA pathway contributes to estrogen-induced proliferation and endocrine resistance of breast cancer cells. Autophagy. 2020;16(6):1061–76.
26. Razidlo GL, Wang Y, Chen J, Krueger EW, Billadeau DD, McNiven MA. Dynamin 2 potentiates invasive migration of pancreatic tumor cells through stabilization of the Rac1 GEF Vav1. Dev Cell. 2013;24(6):573–85.
27. Matsuda Y, Ishiwata T, Yoshimura H, Hagio M, Arai T. Inhibition of nestin suppresses stem cell phenotype of glioblastomas through the alteration of post-translational modification of heat shock protein HSPA8/HSC71. Cancer Lett. 2015;357(2):602–11.
28. Li B, Ming H, Qin S, Zhou L, Huang Z, Jin P, Peng L, Luo M, Zhang T, Wang K et al. HSPA8 Activates Wnt/β-Catenin Signaling to Facilitate BRAF V600E Colorectal Cancer Progression by CMA-Mediated CAV1 Degradation. Adv Sci (Weinheim, Baden-Wurttemberg, Germany). 2024;11(3):e2306535.
29. Yang G, Ma C, Chen Y, Xiang J, Li L, Li Y, Kang L, Liang Z, Yang S. HSPA8 dampens SCAP/INSIG split and SREBP activation by reducing PKR-mediated INSIG phosphorylation. Cell Rep. 2025;44(3):115339.
30. Mi J, Yang Y, Yao H, Huan Z, Xu C, Ren Z, Li W, Tang Y, Fu R, Ge X. Inhibition of heat shock protein family A member 8 attenuates spinal cord ischemia-reperfusion injury via astrocyte NF-κB/NLRP3 inflammasome pathway : HSPA8 inhibition protects spinal ischemia-reperfusion injury. J Neuroinflammation. 2021;18(1):170.
31. Liu J, Song K, Lin B, Chen Z, Liu Y, Qiu X, He Q, Zuo Z, Yao X, Huang X, et al. The suppression of HSPA8 attenuates NLRP3 ubiquitination through SKP2 to promote pyroptosis in sepsis-induced lung injury. Cell Biosci. 2024;14(1):56.
32. Hui W, Song T, Yu L, Chen X. The Binding of HSPA8 and Mitochondrial ALDH2 Mediates Oxygen-Glucose Deprivation-Induced Fibroblast Senescence. Antioxidants (Basel, Switzerland). 2023;13(1):42.

Publisher's Note